


## Room-Temperature Anomalous Inverse Spin Hall Effect in an Easy-Plane Antiferromagnetic Insulator for Néel-Vector Manipulation and Detection

Yupeng Hui<sup>1,2</sup>, Yueying Zhang<sup>1,2</sup>, Yue-Qi Wang<sup>1,2</sup>, Xin Gan<sup>1,2</sup>, Lei Wang<sup>1,2</sup>, Shaoxuan Liu<sup>1,2</sup>, Jincheng Zhang<sup>1,2,3</sup>, Yue Hao<sup>1,2,3</sup> and Haijiao Harsan Ma<sup>1,2,3,\*</sup>

<sup>1</sup>Low Dimensional Quantum Physics & Device Group, School of Microelectronics, Xidian University, 2 South Taibai Road, Xi'an 710071, China

<sup>2</sup>State Key Discipline Laboratory of Wide Band Gap Semiconductor Technology, School of Microelectronics, Xidian University, 2 South Taibai Road, Xi'an 710071, China

<sup>3</sup>Collaborative Innovation Center of Quantum Information of Shaanxi Province, Xidian University, Xi'an 710071, China

 (Received 18 January 2022; revised 14 June 2022; accepted 28 July 2022; published 13 September 2022)

Metallic antiferromagnets are demonstrated to show an unconventional spin Hall effect (SHE) and the inverse spin Hall effect (ISHE), which are very promising for Néel-vector detection. However, the ISHE is absent in insulating antiferromagnets, as it does not conduct charge current. Here, we report our observation of the anomalous ISHE at the interface of the easy-plane insulator antiferromagnetic nickel oxide and the heavy metal platinum. We find that, at the interface of NiO/Pt, the ISHE generates an anomalous hysteretic transverse voltage in both Hall and planar Hall measurements, depending on spin-current propagation and the polarization direction. The observation of a nonzero transverse voltage in Pt indicates the appearance of a spin current with longitudinal polarization reflected from NiO, implying Néel-vector reorientation from the transverse to longitudinal direction. Our simulation indicates that the Néel vector can be reoriented by a spin current injected from the heavy metal and an applied magnetic field. The observed anomalous ISHE permits the manipulation and detection of the Néel order in insulating antiferromagnets.

DOI: [10.1103/PhysRevApplied.18.034032](https://doi.org/10.1103/PhysRevApplied.18.034032)

Antiferromagnets (AFMs) have drawn intensive attention in spintronics for their advantages, such as ultrafast signal generation, characteristic symmetry breaking, and resultant emergent spin functionalities due to their unique magnetic order [1–8]. Control and readout of the antiferromagnetic order parameter the Néel vector is a critical issue for AFM-based spintronics, although it is still challenging [9]. So far, different methods, including spin- or current-induced torques and magnetoelectric and magnetoelastic coupling, have been used to control the Néel vector [10–12]. Furthermore, spin Hall magnetoresistance and the inverse spin Hall effect (ISHE), as well as optical or electrical imaging methods, have been developed to detect the Néel vector [1,13].

Recently, it has been shown that a spin current generated by the spin hall effect (SHE) can be very efficient at manipulating the Néel vector [14–21]. Detecting spin dynamics in antiferromagnetic insulators (AFMI) by the ISHE in the proximity of a heavy metal (HM) is an established method involving the spin Seebeck effect [22,23] or spin Hall magnetoresistance [24]. Injection of a charge current into the HM layer [17,25] generates a spin current through the SHE

and transmits a pure spin current to an adjacent AFMI through the AFMI/HM interface [18,26,27]. The injected spin current interacts with the Néel vector, and spin current with polarization parallel to the Néel vector can be reflected back to the HM layer in the AFMI. The reflected spin current generates a voltage in the direction perpendicular to spin polarization via the ISHE, providing an electrical readout of the Néel vector in the AFMI. In fact, Néel vectors in the AFMI tend to be aligned along the current direction [28] but perpendicular to the magnetic field [29]. Thus, a prospective approach to realize simultaneous manipulation and detection of the Néel vector is to measure the field-dependent ISHE in the HM layer.

In Hall measurements, a transverse voltage,  $\Delta V_{xy}$ , is measured as a function of magnetic field with a longitudinal current in Hall bar patterned devices (Fig. 1). Typically, a transverse voltage,  $\Delta V_{xy}$ , can originate from spin Hall magnetoresistance, the Hall effect, or the planar Hall effect in the presence of a magnetic field; the anomalous Hall effect in the presence of magnetization; the inverse spin Hall effect in the presence of a spin current; and the Seebeck effect due to a thermal gradient. Regardless of details of the mechanisms generating  $\Delta V_{xy}$ , it is established that detecting a transverse voltage,  $\Delta V_{xy}$ , is a reliable method for detection of the orientation of the Néel

\*mahj07@xidian.edu.cn

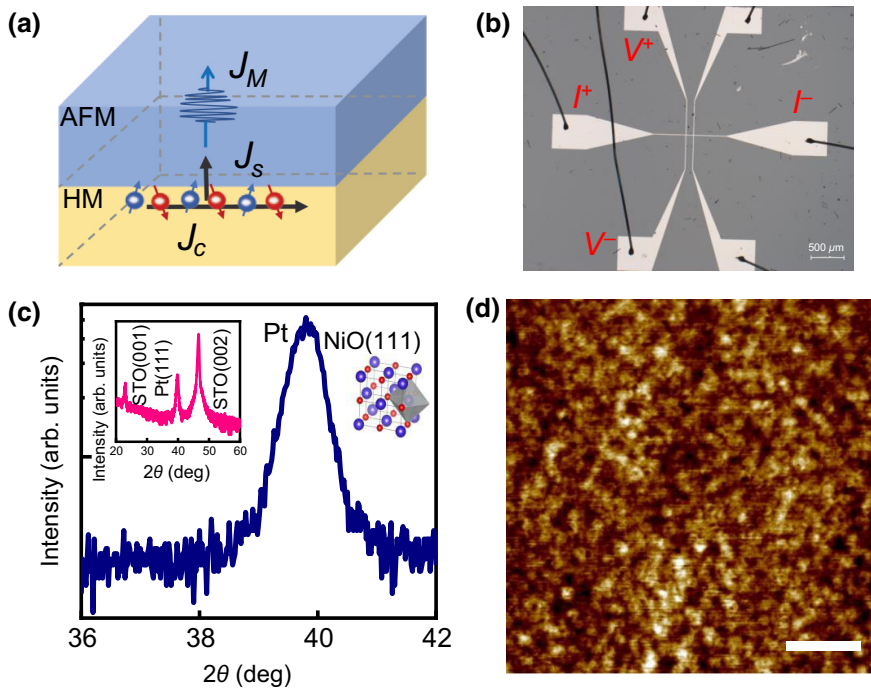


FIG. 1. Experimental setup and device structure for ISHE measurements and Néel-vector detection. (a) Layout of the sample structure with HM and AFMs. Charge current,  $J_c$ , is applied to the HM layer, which generates a spin current,  $J_s$ , flow along the  $z$  direction, transforming into a magnon current  $J_M$  in NiO. (b) Optical image of the device. (c) X-ray reflection data (XRD) on NiO/Pt/SrTiO<sub>3</sub>(001) around the  $\langle 111 \rangle$  reflection of Pt(111) film on SrTiO<sub>3</sub> substrate. Left inset shows the wide-angle XRD data. Right inset shows the crystallographic structure of NiO(111). (d) Atomic force microscopy image of the NiO/Pt(111) film with 20-nm Pt. Size of the white scale bar is 200 nm. Roughness is 0.216 nm.

vector in an AFM. In fact, a transition between zero and nonzero Hall voltages is observed in Néel-vector rotation in an antiferromagnet [30].

Here, we observe the magnetic-field-dependent anomalous ISHE at the interface of an insulating easy-plane antiferromagnet, NiO, and a HM Pt layer, which reflects the injected spin-current-controlled Néel-vector rotation in the AFM. NiO has a simple face-centered-cubic structure and possesses Ni<sup>2+</sup> ions, which are ferromagnetically ordered in the  $\{111\}$  planes and antiferromagnetically ordered in adjacent planes at room temperature. Differ from easy-axis antiferromagnets, such as MnF<sub>2</sub>, NiO has a hard axis along  $\langle 111 \rangle$  and an easy axis along  $\langle 11-2 \rangle$ , called hard-axis or easy-plane antiferromagnets, respectively [8,26]. The Pt layer is used to generate a spin current and transmit to the top AFM layer [Fig. 1(a)] [15,31,32]. The injected pure spin current in NiO interacts with antiferromagnetically ordered sublattice magnetization, which results in the reorientation of Néel vectors. The reorientation of the Néel vector in an AFM generates a change of the reflected spin polarization at the NiO/Pt interface, leading to a change of the transverse-voltage signal via the ISHE in Pt [33,34]. Figure 1(b) shows an optical image of one of the devices. Pt layers are (111) orientated [Fig. 1(c)] with a smooth surface of the top NiO layer [Fig. 1(d)].

Figure 2 shows our main results for the field-dependent anomalous ISHE at the interface of NiO/Pt as a function of out-of-plane magnetic field for a sample with 5-nm NiO on 15-nm Pt. The transverse Hall resistance,  $R_{xy}$ , clearly shows anomalous hysteretic behavior, deviating from that of conventional Hall resistance, which is linear with respect to the magnetic field. Interestingly, the

magnetic-field-dependent Hall resistance measured at a large current (3 mA) is linear, as shown by dark lines, which is consistent with a conventional Hall effect. This indicates that anomalous transverse Hall resistance appears

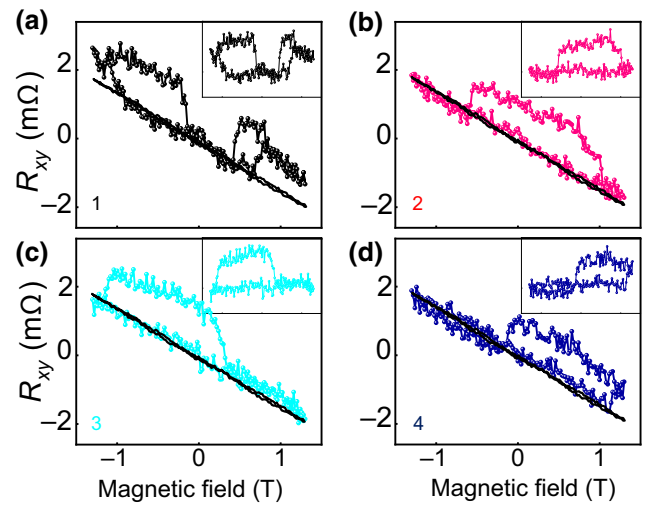


FIG. 2. Anomalous transverse-voltage signal in NiO/Pt under an out-of-plane magnetic field. (a)–(d) Four types of magnetic-field-dependent Hall resistance measured in the Hall bar device at room temperature. Hall resistance data shown are for sample B [NiO(5)/Pt(15 nm)] under a current of 500  $\mu$ A. Insets show the hysteric transverse-voltage signal after subtracting normal Hall resistance data. Dark lines are linear Hall resistance measured with 3 mA without loops. 1, a pair of loops at positive and negative magnetic fields (a); 2, a nearly symmetric loop (b); 3 (c) and 4 (d), asymmetric loop.

only for a small current and is absent for a large current. There are mainly four types of anomalous transverse Hall resistance (indicated by black, pink, cyan, and blue solid dots) observed in a few hundred measurement scans. The first type (1) shows a hysteresis with a pair of loops [Fig. 2(a), dark]; the second type (2) [Fig. 2(b), red], third type (3) [Fig. 2(c), cyan], and fourth type (4) [Fig. 2(d), olive] have single loops. The insets in Fig. 2 show  $\Delta V_{xy}$  after subtracting the normal Hall signal (dark lines) (see Note 1 within the Supplemental Material [43]). As we mention, NiO is insulating; thus, the Hall voltages measured are from the Pt layer. The appearance of an anomalous transverse voltage originates from the NiO/Pt interface.

The observed anomalous hysteretic transverse voltage has several possible mechanisms. (1) Spin Hall magnetoresistance. (2) The Hall effect; an out-of-plane net magnetization is within the scope of the Hall effect, similar to the anomalous Hall effect in ferromagnetic systems. In this case, the observed zero and nonzero values of anomalous transverse-voltage signals correspond to switching *on* and *off* of the out-of-plane net magnetization. (3) The ISHE; a spin current with polarization along the  $x$  direction and propagating direction along the  $z$  direction can generate an additional transverse voltage via the ISHE at the interface. (4) A thermal temperature gradient in the case of the Seebeck effect; as a hysteretic transverse loop is unexpected in spin Hall magnetoresistance and the Seebeck effect, a possible mechanism should be either the Hall effect with an emergent net magnetization moment or the ISHE in the

presence of an emergent spin current with different polarizations. A net magnetization moment in NiO appears in the spin-flop state when the two antiparallel-aligned sublattice moments rotate along the magnetic field; in this case, one would expect the net magnetization moment to reverse sign when the magnetic field changes direction, thus the transverse voltage should reverse sign, as in the anomalous Hall effect. This suggests that the Hall effect is very unlikely to be the origin of data shown in Fig. 2.

We further investigate the field-dependent transverse voltage in Hall effect measurements with an out-of-plane magnetic field and a planar Hall effect measurement with an in-plane magnetic field for different samples, as shown in Fig. 3. The thickness of NiO is fixed to 5 nm with thicknesses of Pt of 20, 15, and 10 nm. All four sets of data (1, 2, 3, and 4) can be observed for all the samples, and we show data sets 1 and 2 here. The left (right) panel shows anomalous transverse voltages of data sets 1 and 2 with an out-of-plane (in-plane) magnetic field for three different samples. We notice that the slope of the transverse voltage in Hall measurements with an out-of-plane field is much steeper than the slope in planar Hall measurements with an in-plane field. It seems that there could be some correlations between the observed linear voltage increase in the planar Hall effect shown in Fig. 3(b) and the previously reported intrinsic ordinary magnetoresistance of Pt [41].

The long-range magnetic order in NiO results from the superexchange interaction that favors antiparallel alignment between neighboring sublattice magnetizations ( $\mathbf{M}_1$  and  $\mathbf{M}_2$ ) in the  $\{111\}$  planes. The Néel order,

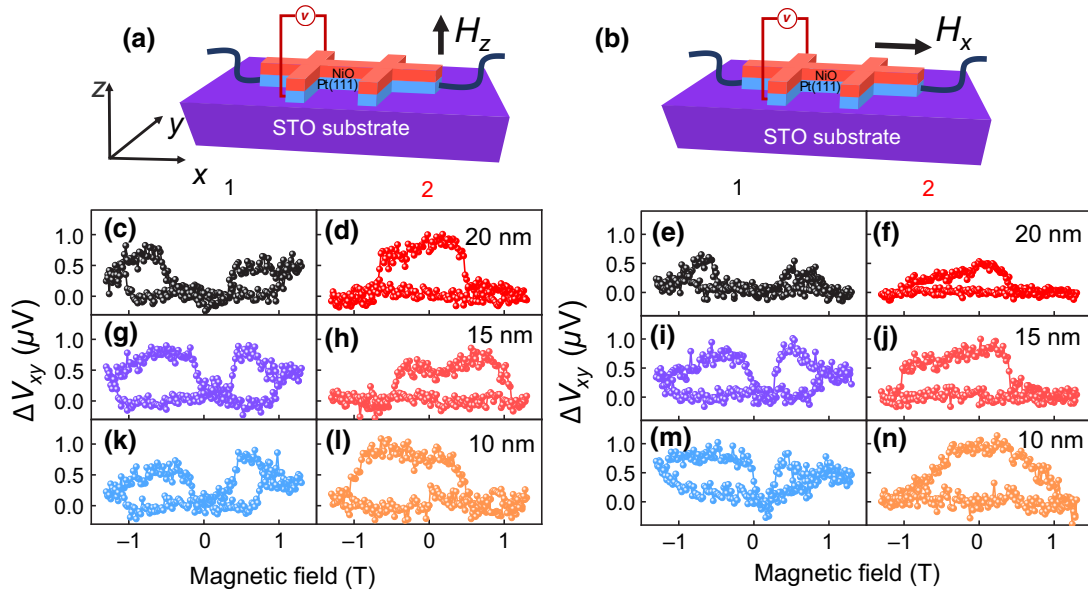


FIG. 3. Anomalous inverse spin Hall voltages under out-of-plane and in-plane magnetic fields. Left panel, measurement scheme with out-of-plane magnetic field,  $H_z$ , is shown in (a). Anomalous ISHE is shown in (c),(d) for sample C (20 nm); (g),(h) for sample B (15 nm); and (k),(l) for sample A (10 nm). Right panel, measurement scheme with in-plane magnetic field,  $H_x$ , is shown in (b). Anomalous ISHE shown in (e),(f) for sample C (20 nm); (i),(j) for sample B (15 nm); and (m),(n) for sample A (10 nm).

$\mathbf{L} = \mathbf{M}_1 - \mathbf{M}_2$ , is rotated by the antidampinglike torque,  $\mathbf{T}_{1,2} \sim \mathbf{M}_{1,2} \times (\mathbf{M}_{1,2} \times \mathbf{J}_s)$ , due to spin current, acting as an effective field [9] (see Note 2 within the Supplemental Material [43]). In an easy-plane AFMI such a field is staggered, namely, alternating in sign between sublattices and the staggered fields can efficiently manipulate the AFMI. Unlike spin-transfer torque, the torque induced by spin current is expected to be much more robust against disorder, and it would be able to rotate the Néel vector.

As previously mentioned, the Néel vector tends to align with the direction perpendicular to the magnetic field and parallel to the current. Pt is (111) orientated in our samples [Fig. 1(c)]; thus, the sample plane (in-plane) is the easy plane in which the Néel vectors are located. When no magnetic field is applied, the SHE-induced spin current,  $J_{zy}^s$ , with polarization along  $y$  and the propagating direction along  $z$  is generated at the NiO/Pt interface. No transverse voltage is expected in this case. As the Néel vector prefers to be aligned perpendicular to the magnetic field, the Néel vector is rotated to the longitudinal  $x$  direction with increasing out-of-plane magnetic field under certain conditions. A nonzero transverse voltage is expected in this case. However, as the magnetic field is reduced toward zero, the spin current  $J_{zy}^s$ , with polarization along  $y$  induced by the SHE appears again; thus, the transverse voltage decreases with reducing field and disappears at some point. Thus, the jump of the transverse voltage from zero to nonzero indicates rotation of the Néel vector from the  $y$  to  $x$  direction and vice versa. With an applied in-plane magnetic field, there are two opposite torques on the Néel vector from the current and magnetic field, leading to competing Néel vectors along the  $x$  and  $y$  directions. In this case, an antiferromagnet with multidomains is preferred [40], and a gradual change of  $x$ - and  $y$ -orientated AFM domains is expected, which is consistent with shallower slopes in the planar Hall measurements (Fig. 3).

We next investigate the current-dependent anomalous transverse voltage, as shown in Fig. 4. We notice that a minimum current of about  $300 \mu\text{A}$  is needed to observe a stable anomalous transverse voltage, while no visible

anomalous transverse voltage is observed for currents above  $3 \text{ mA}$  [Fig. 4(g)]. The maximum transverse-voltage signal appears at around  $750 \mu\text{A}$  for all three samples. This is consistent with our analysis that there are two different torques on the Néel vector from both the current and magnetic field. Considering the appearance of hysteretic transverse-voltage loops, as well as the absence of an anomalous transverse voltage above  $3 \text{ mA}$ , the origin of the transverse-voltage signal is mainly from the ISHE.

When a charge current,  $J_c$ , is injected along the  $x$  direction, a spin current,  $J_{zy}^s$ , is generated in Pt due to the SHE with polarization along  $y$  and the propagating direction along  $z$ , obeying  $J^s = \hbar/2e\theta_{\text{SH}}J_cp$ , where  $\theta_{\text{SH}}$  is the spin Hall angle of Pt and  $p$  is the polarization of the spin current. Unlike the SHE in ferromagnets and heavy metals, in which spin polarization, the spin-propagating direction, and charge-flow direction are all orthogonal [3,4], the spin current generated in antiferromagnets can have polarization parallel to the spin-current propagating or charge-flow direction, e.g.,  $J_{zz}^s, J_{zx}^s$ , and  $J_{zy}^s$  [2,35], as observed in the antiferromagnetic SHE in manganese [1,2,35]. As the Néel vector prefers to be aligned with the current but perpendicular to the magnetic field, the spin current with polarization in the  $x$ - $y$  plane and propagating along the  $z$  direction injected from Pt into NiO will be reflected back to the NiO/Pt interface in NiO. Namely, spin current  $J_{zy}^s$  in the case of the Néel vector along  $y$  or  $J_{zx}^s$  for the Néel vector along  $x$ , can be reflected in NiO while others will be scattered and dissipated [Figs. 5(a) and 5(b)]. The reflected spin current transforms into a voltage signal via the ISHE at the NiO/Pt interface. A nonzero transverse voltage is possible in the presence of spin current  $J_{zx}^s$ , indicating a Néel vector along the  $x$  direction. Notably, in the case of a certain magnon excited in the AFMI NiO, it is possible to generate an oscillating moment along the  $x$  direction in NiO, generating a nonzero transverse voltage at the NiO/Pt interface. This is possibly the case for data sets 2–4, with big loops in Figs. 2 and 3. If there is a net out-of-plane magnetization in an AFMI, e.g., in a spin-flop state, a nonzero transverse voltage is also possible. However, this

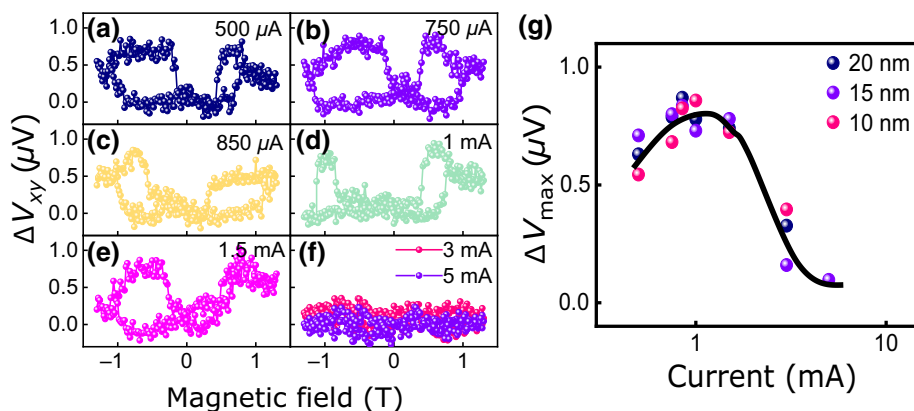


FIG. 4. Current-dependent anomalous inverse spin Hall voltage signals. Type-1 transverse hysteretic loops appear for applied currents below  $3 \text{ mA}$  (a)–(e), while they are absent for currents larger than  $3 \text{ mA}$  (f). (g) Maximum value of magnonic inverse spin Hall voltage signal,  $\Delta V_{\text{max}}$ , as a function of applied current for all samples. Dark line is a guide to the eye.



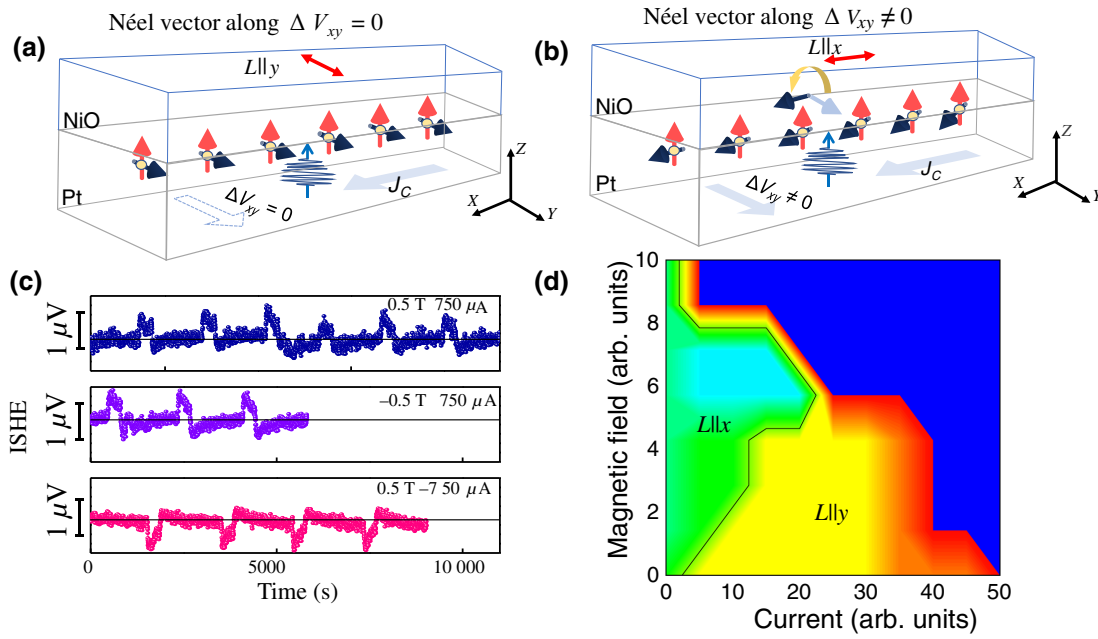


FIG. 5. Mechanism of anomalous transverse voltage and electrical detection of Néel-vector reorientation in easy-plane AFMI NiO via the ISHE. (a),(b) Schematic picture of the mechanism of the origin of nonzero (zero) transverse voltage via the ISHE induced by a spin current polarized along the  $x$  ( $y$ ) direction with a propagating direction from NiO to the Pt interface. (c) ISHE as a function of time under different magnetic fields and applied currents. Top, current  $750 \mu\text{A}$ , out-of-plane magnetic field  $0.5 \text{ T}$ ; middle, current  $750 \mu\text{A}$ , out-of-plane magnetic field  $-0.5 \text{ T}$ ; bottom, current  $-750 \mu\text{A}$ , out-of-plane magnetic field  $0.5 \text{ T}$ . (d) Simulated phase diagram of the Néel vector in easy-plane AFMI NiO.  $L||x$  indicates the Néel vector with a dominating component along the longitudinal  $x$  direction (green area), while  $L||y$  indicates the Néel vector with a component along the transverse  $y$  direction (yellow). In the spin-flop state, a net magnetization moment exists (red and blue area). Initial sublattice moment is along the easy axis, with current along the  $x$  direction and an applied out-of-plane magnetic field; resultant Néel vector is recorded for each point.

requires a large externally applied magnetic field or applied charge current. We observe data set 2 with big hysteresis loops for a small current and small magnetic field; thus, this situation is highly unlikely in the scope of our experiments. Thus, we conclude that the observed anomalous transverse voltage is generated via the ISHE at the NiO/Pt interface.

One remarkable observation is resonance peaks in the time-dependent anomalous ISHE under positive and negative magnetic fields with the charge currents shown in Fig. 5(c). The anomalous ISHE signal reverses sign upon reversing the direction of the applied current, while reversing the direction of the magnetic field does not lead to similar results, indicating the crucial role of the spin current injected via the SHE. The periodicity varies with applied field and current. In the experiment, a pulse current is applied with a duration of about  $1 \mu\text{s}$  and an interval of about  $1 \text{ ms}$ . With spin polarization accumulating, the Néel vector can be rotated to the  $x$  direction at a certain threshold with increasingly accumulated spin polarization and finally induces a transverse-voltage signal. Interestingly, the generated ISHE signal slowly decays as a function of time and the process repeats. This fits well with a multidomain scenario. The thermomagnetoelastic switching mechanism combined with thermal excitations can have

possible contributions for the observed transverse-voltage-signal variation [12]. Figure 5(d) shows the calculated phase diagram for NiO under a current and out-of-plane magnetic field along the hard axis (see Note 3 within the Supplemental Material [43]). When the current slowly increases, there can be a Néel vector along the  $y$  direction. With both current and magnetic field applied, the Néel vector can be aligned along the  $x$  direction. The change of the Néel vector is dynamic and a magnon can exit to assist reorientation of the Néel vector [21] (see Methods and Note 2 within the Supplemental Material [43]). The alignment of spin current along the Néel vector and reflection of spin current from the antiferromagnet can be related to the existence of different magnon modes [39]. Hysteretic transverse voltages of types 2–4 with big loops show nonzero values at zero magnetic field, indicating the presence of spin current  $J_{zx}^s$  with polarization along the  $x$  direction required by the ISHE; thus, in this case, spin current  $J_{zy}^s$  is rotated to  $J_{zx}^s$  in NiO, which is consistent with the presence of excited magnon modes in the AFMI.

The spin-current-induced anomalous ISHE requires a current of  $300 \mu\text{A}$  [Fig. 3(d)], corresponding to a current density of  $2 \times 10^5 \text{ A/cm}^2$  for sample B. For comparison, the reported current-induced Néel-vector switching requires a current around  $10^7 \text{ A/cm}^2$  [18–20],

about 2 orders of magnitude higher than our experiment. This indicates that external-magnetic-field-assisted Néel-order switching by utilizing a pure spin current is much more efficient, less power consuming, and avoids Joule heating (see Note 4 and Fig. S8 within the Supplemental Material [43]). When the charge current is too large, torque generated by the spin current is so strong that it makes reorientation of the Néel vector more difficult, leading to the disappearance of hysteretic transverse-voltage loops.

We finally remark that the surface of the Pt thin film can be made ferromagnetic, depending on the interface conditions [36], and there can be an exchange bias between the antiferromagnetic order in NiO and induced ferromagnetism at the interface of NiO/Pt [37]. In this case, one would expect to observe an anomalous Hall effect with an exchange bias. Notably, the magnetic proximity effect [36, 37] or thermomagnetoelastic effects [12] can be present in our system, although the effects are insignificant. However, data sets 1 and 4 show a shift of the hysteresis loops by about 0.6–0.7 T from the zero field, which is too large for the exchange bias in NiO at room temperature, compared to the exchange bias in ferromagnet/NiO bilayer systems [38]. We notice that NiO can be in the spin-flop phase [21] under certain conditions with large spin currents and magnetic field, and thus, the observation of the anomalous Hall effect with a small exchange bias (see Fig. S9 within the Supplemental Material [43]) is possible. In contrast, the anomalous ISHEs in data sets 1, 2, 3, and 4 are due to spin-current-induced Néel-vector switching in antiferromagnetic NiO and can only be observed within a certain current range with a maximum transverse voltage value at current of about 750  $\mu$ A (Fig. 4), which is consistent with theoretical simulations [42]. Regarding switching of the Néel vector with current and an out-of-plane magnetic field [big loops, such as data set 2 in Fig. 2(b)], a possible approach is to excite the so-called alpha-magnon mode in NiO [39], which can rotate the Néel vector to the longitudinal direction and have a nonzero oscillating longitudinal polarization, leading to a transverse-ISHE voltage.

In summary, we observe an anomalous ISHE at the interface of the easy-plane AFMI NiO and Pt. The anomalous ISHE can be manipulated by charge current and magnetic field and originates from rotation of the Néel vector in an antiferromagnet. This provides us an effective approach to manipulate and detect the Néel order in an otherwise AFMI, facilitating the achievement of high-quality antiferromagnetic memory devices.

Data are available upon reasonable request from the corresponding authors.

#### ACKNOWLEDGMENTS

We thank the National Science Foundation (NSF) of China Grant No. 61904140 for financial support. This work is supported by the National Key

Research and Development Program of China (Grant No. 2021YFA0715600) and “the Fundamental Research Funds for the Central Universities” (Grant No. JC2101). The authors acknowledge W. Ning, J. H. Zhou, and G. L. Cheng for help with additional transport measurements.

- 
- [1] M. Kimata, H. Chen, K. Kondou, S. Sugimoto, P. K. Muduli, M. Ikhlas, Y. Omori, T. Tomita, A. H. MacDonald, S. Nakatsuji, and Y. Otani, Magnetic and magnetic inverse spin Hall effects in a non-collinear antiferromagnet, *Nature* **565**, 627 (2019).
  - [2] X. Chen, *et al.*, Observation of the antiferromagnetic spin Hall effect, *Nat. Mater.* **20**, 800 (2021).
  - [3] Y. K. Kato, R. C. Myers, A. C. Gossard, and D. D. Awschalom, Observation of the spin Hall effect in semiconductors, *Science* **306**, 1910 (2004).
  - [4] J. E. Hirsch, Spin Hall Effect, *Phys. Rev. Lett.* **83**, 1834 (1999).
  - [5] T. Kimura, Y. Otani, T. Sato, S. Takahashi, and S. Maekawa, Room-Temperature Reversible Spin Hall Effect, *Phys. Rev. Lett.* **98**, 156601 (2007).
  - [6] O. Gomonay, V. Baltz, A. Brataas, and Y. Tserkovnyak, Antiferromagnetic spin textures and dynamics, *Nat. Phys.* **14**, 213 (2018).
  - [7] T. Jungwirth, J. Sinova, A. Manchon, X. Marti, J. Wunderlich, and C. Felser, The multiple directions of antiferromagnetic spintronics, *Nat. Phys.* **14**, 200 (2018).
  - [8] H. Qiu, L. Zhou, C. Zhang, J. Wu, Y. Tian, S. Cheng, S. Mi, H. Zhao, Q. Zhang, D. Wu, *et al.*, Ultrafast spin current generated from an antiferromagnet, *Nat. Phys.* **17**, 388 (2021).
  - [9] J. Železný, P. Wadley, K. Olejník, A. Hoffmann, and H. Ohno, Spin transport and spin torque in antiferromagnetic devices, *Nat. Phys.* **14**, 220 (2018).
  - [10] J. Železný, H. Gao, K. Výborný, J. Zemen, J. Mašek, A. Manchon, J. Wunderlich, J. Sinova, and T. Jungwirth, Relativistic Néel-Order Fields Induced by Electrical Current in Antiferromagnets, *Phys. Rev. Lett.* **113**, 157201 (2014).
  - [11] F. Zheng, M. Zhu, X. Li, P. Zhang, J. Liu, J. Dong, and J. Zhang, Ferroelectric control of the Néel vector in *L10*-type antiferromagnetic films, *Phys. Rev. B* **104**, 144403 (2021).
  - [12] H. Meer, F. Schreiber, C. Schmitt, R. Ramos, E. Saitoh, O. Gomonay, J. Sinova, and M. Kläui, Direct imaging of current-induced antiferromagnetic switching revealing a pure thermomagnetoelastic switching mechanism in NiO, *Nano Lett.* **21**, 114 (2021).
  - [13] S. Bodnar, L. Šmejkal, I. Turek, T. Jungwirth, O. Gomonay, J. Sinova, A. Sapozhnik, H. Elmers, M. Kläui, and M. Jourdan, Writing and reading antiferromagnetic  $Mn_2Au$  by Néel spin-orbit torques and large anisotropic magnetoresistance, *Nat. Commun.* **9**, 348 (2018).
  - [14] E. Saitoh, M. Ueda, H. Miyajima, and G. Tatara, Conversion of spin current into charge current at room temperature: Inverse spin-Hall effect, *Appl. Phys. Lett.* **88**, 182509 (2006).
  - [15] T. Jungwirth, X. Marti, P. Wadley, and J. Wunderlich, Antiferromagnetic spintronics, *Nat. Nanotechnol.* **11**, 231 (2016).

- [16] H. Gomonay and V. Loktev, Spin-polarized current-induced instability in the spin-valve antiferromagnetic layer, *J. Magn. Soc. Japan* **32**, 535 (2008).
- [17] T. Tanaka, H. Kontani, M. Naito, T. Naito, D. S. Hirashima, K. Yamada, and J. Inoue, Intrinsic spin Hall effect and orbital Hall effect in  $4d$  and  $5d$  transition metals, *Phys. Rev. B* **77**, 165117 (2008).
- [18] T. Moriyama, K. Oda, T. Ohkochi, M. Kimata, and T. Ono, Spin torque control of antiferromagnetic moments in NiO, *Sci. Rep.* **8**, 14167 (2018).
- [19] X. Chen, R. Zarzuela, J. Zhang, C. Song, X. Zhou, G. Shi, F. Li, H. Zhou, W. Jiang, F. Pan, and Y. Tserkovnyak, Antidamping-Torque-Induced Switching in Biaxial Antiferromagnetic Insulators, *Phys. Rev. Lett.* **120**, 207204 (2018).
- [20] Y. Wang, D. Zhu, Y. Yang, K. Lee, R. Mishra, G. Go, S.-H. Oh, D.-H. Kim, K. Cai, E. Liu, *et al.*, Magnetization switching by magnon-mediated spin torque through an antiferromagnetic insulator, *Science* **366**, 1125 (2019).
- [21] P. Vaidya, S. A. Morley, J. V. Tol, Y. Liu, R. Cheng, A. Brataas, D. Lederman, and E. D. Barco, Subterahertz spin pumping from an insulating antiferromagnet, *Science* **368**, 160 (2020).
- [22] H. Chen, Q. Niu, and A. H. MacDonald, Anomalous Hall Effect Arising from Noncollinear Antiferromagnetism, *Phys. Rev. Lett.* **112**, 017205 (2014).
- [23] W. Zhang, M. B. Jungfleisch, W. Jiang, J. E. Pearson, A. Hoffmann, F. Freimuth, and Y. Mokrousov, Spin Hall Effects in Metallic Antiferromagnets, *Phys. Rev. Lett.* **113**, 196602 (2014).
- [24] S. M. Wu, W. Zhang, K. C. Amit, P. Borisov, J. E. Pearson, J. S. Jiang, D. Lederman, A. Hoffmann, and A. Bhattacharya, Antiferromagnetic Spin Seebeck Effect, *Phys. Rev. Lett.* **116**, 097204 (2016).
- [25] G. Y. Guo, S. Murakami, T.-W. Chen, and N. Nagaosa, Intrinsic Spin Hall Effect in Platinum: First-Principles Calculations, *Phys. Rev. Lett.* **100**, 096401 (2008).
- [26] I. Gray, T. Moriyama, N. Sivadas, G. M. Stiehl, J. T. Heron, R. Need, B. J. Kirby, D. H. Low, K. C. Nowack, D. G. Schlom, *et al.*, Spin Seebeck Imaging of Spin-Torque Switching in Antiferromagnetic Pt/NiO Heterostructures, *Phys. Rev. X* **9**, 041016 (2019).
- [27] Y. Kajiwara, K. Harii, S. Takahashi, J. Ohe, K. Uchida, M. Mizuguchi, H. Umezawa, H. Kawai, K. Ando, K. Takanashi, *et al.*, Transmission of electrical signals by spin-wave interconversion in a magnetic insulator, *Nature* **464**, 262 (2010).
- [28] C. Schmitt, L. Baldrati, L. Sanchez-Tejerina, F. Schreiber, A. Ross, M. Filianina, S. Ding, F. Fuhrmann, R. Ramos, F. Maccherozzi, *et al.*, Identification of Néel Vector Orientation in Antiferromagnetic Domains Switched by Currents in NiO/Pt Thin Films, *Phys. Rev. Appl.* **15**, 034047 (2021).
- [29] W. L. Roth, Neutron and optical studies of domains in NiO, *J. Appl. Phys.* **31**, 2000 (1960).
- [30] A. Mahmood, W. Echtenkamp, M. Street, J.-L. Wang, S. Cao, T. Komesu, P. A. Dowben, P. Buragohain, H. Lu, A. Gruverman, *et al.*, Voltage controlled Néel vector rotation in zero magnetic field, *Nat. Commun.* **12**, 1674 (2021).
- [31] T. Moriyama, S. Takei, M. Nagata, Y. Yoshimura, N. Matsuzaki, T. Terashima, Y. Tserkovnyak, and T. Ono, Antidamping spin transfer torque through epitaxial nickel oxide, *Appl. Phys. Lett.* **106**, 162406 (2015).
- [32] M. W. Daniels, W. Guo, G. M. Stocks, D. Xiao, and J. Xiao, Spin-transfer torque induced spin waves in antiferromagnetic insulators, *New J. Phys.* **17**, 103039 (2015).
- [33] A. Hoffmann, Spin Hall effects in metals, *IEEE Trans. Magn.* **49**, 5172 (2013).
- [34] W. Lin and C. L. Chien, Electrical Detection of Spin Backflow from an Antiferromagnetic Insulator/Y<sub>3</sub>Fe<sub>5</sub>O<sub>12</sub> Interface, *Phys. Rev. Lett.* **118**, 067202 (2017).
- [35] T. Nan, *et al.*, Controlling spin current polarization through non-collinear antiferromagnetism, *Nat. Commun.* **11**, 4671 (2020).
- [36] Y. Sakamoto, Y. Oba, H. Maki, M. Suda, Y. Einaga, T. Sato, M. Mizumaki, N. Kawamura, and M. Suzuki, Ferromagnetism of Pt nanoparticles induced by surface chemisorption, *Phys. Rev. B* **83**, 104420 (2011).
- [37] H. Wu, C. Wan, Z. Yuan, X. Zhang, J. Jiang, Q. Zhang, Z. Wen, and X. Han, Observation of pure inverse spin Hall effect in ferromagnetic metals via ferromagnetic/antiferromagnetic exchange-bias structures, *Phys. Rev. B* **92**, 054404 (2015).
- [38] Y. Gao, H. Sakimura, H. Gao, T. Gao, J. Wang, K. Ando, T. Harumoto, Y. Nakamura, and J. Shi, Perpendicular exchange bias independent of NiO layer thickness in NiO/CoPt structures with orthogonal spin configuration, *J. Phys. D: Appl. Phys.* **53**, 225002 (2020).
- [39] S. M. Rezende, A. Azevedo, and R. L. Rodríguez-Suárez, Introduction to antiferromagnetic magnons, *J. Appl. Phys.* **126**, 151101 (2019).
- [40] S. Mandal, K. S. R. Menon, F. Maccherozzi, and R. Belkhou, Strain-induced nonequilibrium magnetoelastic domain structure and spin reorientation of NiO(100), *Phys. Rev. B* **80**, 184408 (2009).
- [41] L. Baldrati, A. Ross, T. Niizeki, C. Schneider, R. Ramos, J. Cramer, O. Gomonay, M. Filianina, T. Savchenko, D. Heinze, *et al.*, Full angular dependence of the spin Hall and ordinary magnetoresistance in epitaxial antiferromagnetic NiO(001)/Pt thin films, *Phys. Rev. B* **98**, 024422 (2018).
- [42] Ø Johansen and A. Brataas, Spin pumping and inverse spin Hall voltages from dynamical antiferromagnets, *Phys. Rev. B* **95**, 220408(R) (2017).
- [43] See the Supplemental Material at <http://link.aps.org/supplemental/10.1103/PhysRevApplied.18.034032> for sample fabrication, transport measurements, theoretical simulations, and additional data to support the work.